

Spectral evolution of GRB 060904A observed with *Swift* and *Suzaku*

— Possibility of Inefficient Electron Acceleration

Daisuke YONETOKU,^{1,14} Sachiko TANABE,¹ Toshio MURAKAMI,¹ Naomi EMURA,¹ Yuka AOYAMA,¹ Takashi KIDAMURA,¹ Hironobu KODAIRA,¹ Yoshiki KODAMA,¹ Ryota KOZAKA,¹ Takuro NASHIMOTO,¹ Shinya OKUNO,¹ Satoshi YOKOTA,¹ Satoru YOSHINARI,¹ Keiichi ABE,² Kaori ONDA,² Makoto S. TASHIRO,² Yuji URATA,² Yujin E. NAKAGAWA,³ Satoshi SUGITA,³ Kazutaka YAMAOKA,³ Atsumasa YOSHIDA,³ Takuto ISHIMURA,⁴ Nobuyuki KAWAI,⁴ Takashi SHIMOKAWABE,⁴ Kenzo KINUGASA,⁵ Takayoshi KOHMURA,⁶ Kaori KUBOTA,⁷ Kei SUGIYASU,⁷ Yoshihiro UEDA,⁷ Kensuke MASUI,⁸ Kazuhiro NAKAZAWA,⁸ Tadayuki TAKAHASHI,⁸ Shouta MAENO,⁹ Eri SONODA,⁹ Makoto YAMAUCHI,⁹ Makoto KUWAHARA,^{10,11} Toru TAMAGAWA,^{10,11} Daisuke MATSUURA,¹² Motoko SUZUKI,¹³ Scott BARTHELMY,¹⁴ Neil GEHRELS,¹⁴ and John NOUSEK¹⁵

¹*Department of Physics, Kanazawa University, Kakuma, Kanazawa, Ishikawa 920-1192, Japan
yonetoku@astro.s.kanazawa-u.ac.jp (DY)*

²*Saitama University, Sakura, Saitama 338-8570, Japan*

³*Aoyama Gakuin University, Sagamihara, Kanagawa 229-8558, Japan*

⁴*Tokyo Institute of Technology, Ohokayama, Meguro, Tokyo 152-8551, Japan*

⁵*Gunma Astronomical Observatory, Takayama, Gunma 377-0702, Japan*

⁶*Kogakuin University, Hachioji, Tokyo 192-0015, Japan*

⁷*Kyoto University, Sakyo-ku, Kyoto 606-8502, Japan*

⁸*JAXA/Institute of Space and Astronautical Science, Sagamihara, Kanagawa 229-8510, Japan*

⁹*University of Miyazaki, Gakuen-kibanadai, Miyazaki 889-2192, Japan*

¹⁰*RIKEN, 2-1 Hirosawa, Wako, Saitama 351-0198, Japan*

¹¹*Department of Physics, Tokyo University of Science, 1-3 Kagurazaka, Shinjyuku-ku, Tokyo
162-8601, Japan*

¹²*Osaka University, Toyonaka, Osaka 560-0043, Japan*

¹³*Tsukuba Space Center, 1-1, Sengen 2chome, Tsukuba-city, Ibaraki 305-8505, Japan*

¹⁴*NASA/Goddard Space Flight Center, Greenbelt, MD 20771, USA*

¹⁵*Pennsylvania State University, University Park, PA 16802, USA*

(Received 2000 December 31; accepted 2001 January 1)

Abstract

We observed an X-ray afterglow of GRB 060904A with the *Swift* and *Suzaku*

satellites. We found rapid spectral softening during both the prompt tail phase and the decline phase of an X-ray flare in the BAT and XRT data. The observed spectra were fit by power-law photon indices which rapidly changed from $\Gamma = 1.51_{-0.03}^{+0.04}$ to $\Gamma = 5.30_{-0.59}^{+0.69}$ within a few hundred seconds in the prompt tail. This is one of the steepest X-ray spectra ever observed, making it quite difficult to explain by simple electron acceleration and synchrotron radiation. Then, we applied an alternative spectral fitting using a broken power-law with exponential cutoff (BPEC) model. It is valid to consider the situation that the cutoff energy is equivalent to the synchrotron frequency of the maximum energy electrons in their energy distribution. Since the spectral cutoff appears in the soft X-ray band, we conclude the electron acceleration has been inefficient in the internal shocks of GRB 060904A. These cutoff spectra suddenly disappeared at the transition time from the prompt tail phase to the shallow decay one. After that, typical afterglow spectra with the photon indices of 2.0 are continuously and precisely monitored by both XRT and Suzaku/XIS up to 1 day since the burst trigger time. We could successfully trace the temporal history of two characteristic break energies (peak energy and cutoff energy) and they show the time dependence of $\propto t^{-3} \sim t^{-4}$ while the following afterglow spectra are quite stable. This fact indicates that the emitting material of prompt tail is due to completely different dynamics from the shallow decay component. Therefore we conclude the emission sites of two distinct phenomena obviously differ from each other.

Key words: gamma rays: burst — radiation mechanisms: non-thermal — relativistic jet — X-rays: individual (GRB 060904A) — X-rays: stars acceleration of particles

1. Introduction

Recent *Swift* (Gehrels et al. 2004) observations reveal varying behavior with the early X-ray afterglows of Gamma-ray bursts (GRBs). Nousek et al. (2006) summarized that their X-ray lightcurves can be classified in three basic phases; a very steep decay, a shallow decay and the classical power-law decay, respectively. Additionally, strong X-ray flares during the very steep decay and the shallow decay phases are also found in many early X-ray afterglows.

Jet breaks, as seen in many optical afterglows, have also been observed in X-ray lightcurves (Panaitescu 2007), but Sato et al. (2006) reported that the X-ray afterglow of GRB 050416A lacks its own jet break more than ~ 100 days after the burst trigger time. This fact means that the jet opening half angle must be $\theta \geq 23$ degree, which is much wider than typical opening angles of GRB jets. On the other hand, *Swift* and *Suzaku* combined observations of GRB 060105, Tashiro et al. (2007) found a very early jet break less than 0.04 day after

the GRB trigger time. Therefore we must study these time profiles on a case by case basis. We need much more information about the early X-ray afterglows to comprehend these complex characteristics.

Several authors reported significant spectral softening during the early X-ray afterglows. Especially, Zhang et al. (2006) performed simultaneous spectral analyses for the brightest 17 cases of X-ray afterglows observed by the *Swift*/XRT. In their report, 10 of 17 samples show strong spectral evolution while the others have no evolution. These spectral evolutions are generally explained by a model based on the curvature effect of emitting region (Fenimore et al. 1996; Kumar & Panaitescu 2000; Dermer 2004; Yamazaki et al. 2006). This model implies that the temporal index (α) and the spectral energy index (β) have to show co-evolution as $\alpha = \beta + 2$ for the simplest curvature effect (Liang et al. 2006). However, the observed spectral evolution does not match with the property of temporal decline, so Zhang et al. (2006) introduced another hidden component - the central engine afterglow which may be related to the continuous activity of GRB central engines. These characteristics must be investigated in detail because the cases with spectral softening make up a large fraction of long GRBs.

Using BATSE data, Ryde (2005) investigated the possibility of the existence of thermal emission in the prompt GRB spectra. He proposed a prompt emission spectrum composed of a thermal (blackbody) spectrum combined with a non-thermal (power-law) one. Butler (2006) also explained the anomalous soft X-ray spectrum of GRB 060218 as the thermal plus non-thermal model. He suggested that the X-ray afterglow is dominated by thermal emission with an effective temperature of $kT \sim 0.3$ keV. Even after introducing the thermal blackbody model, the spectral evolution of the power-law component still remains and the photon indices change from $\Gamma = 1.5$ to $\Gamma = 3.4$. Therefore, the thermal model is not sufficient to explain all the spectral softening and additional spectral evolution is required.

In this paper, we show observation results on GRB 060904A with the *Swift* and *Suzaku* satellites. The spectral photon index achieves $\Gamma = 5.30_{-0.59}^{+0.69}$ which is one of the strongest spectral softenings ever observed. In the next section, we summarize X-ray observations with the *Swift* and *Suzaku* satellites for this event. In the third section, we show detailed data reductions for both datasets. We fit two individual models (the single power-law, and a broken power-law with exponential cutoff: BPEC) to the observed spectra. The fitting results and spectral properties are summarized in sections 4 and 5. We succeeded in separating the X-ray afterglow component from the prompt tail and/or X-ray flare. In the 6th section, we show an interesting spectrum during the time when the X-ray afterglow and prompt tail emission co-exist. In the final session, we discuss the observed spectral and temporal properties of GRB 060904A, and we suggest the possible presence of a maximum energy cut-off in the electron energy distribution.

2. Observations

GRB 060904A was detected by the BAT instrument aboard the *Swift* satellite at 2006/09/04 01:03:21 (UT), and localized at R.A. = $15^h50^m58^s$, Dec. = $+44^d57'57''$ (J2000) with an uncertainty of 3 arcminutes. The BAT lightcurve shows several little peaks and then an intense flare composed of multiple spikes at $t - t_{trigger} \sim 55$ sec. Here $t_{trigger}$ is the GRB trigger time. The burst duration time measured in the BAT energy range was about $T_{90} \sim 85$ sec, where T_{90} is measured as the duration of the time interval during which 90 % of the total observed counts have been detected.

The XRT automatically started a follow-up observation from $t - t_{trigger} = 66$ sec in windowed timing mode. A bright X-ray afterglow was found at R.A. = $15^h50^m54^s.9$, Dec. = $+44^d59'07''.8$ (J2000) with an estimated uncertainty of 5.4 arcseconds. The initial flux measured by the first 0.1 sec image was 2.7×10^{-8} erg cm $^{-2}$ s $^{-1}$ (0.2–10 keV band). Unfortunately, *Swift* entered the South Atlantic Anomaly at 01:43:52 (UT), and the XRT observation was interrupted by the next GRB 060904B triggered at 02:31:03 (UT). Therefore XRT data lasted only about 2000 seconds after the burst trigger time.

The X-ray intensity reported by the *Swift*/XRT team was quite bright and also the GRB trigger time satisfied criteria for a target of opportunity (ToO) observation by the Japanese X-ray satellite *Suzaku*. *Suzaku* began the follow-up observation using an HXD nominal pointing mode from 10:29:46 (UT) to 2006/09/05 05:03:46 (UT) with net exposure time of 30.4 ksec. We confirmed the X-ray afterglow found by the *Swift*/XRT within the XIS field of view as shown in figure 2. Therefore *Suzaku* covered the late time behavior of the X-ray afterglow which could not be observed by *Swift*.

No optical counterpart was reported, and this burst was categorized as an optically dark GRB. So we have no direct information about the redshift. The *Subaru* telescope observed the field of GRB 060904A with the MOIRCS near-infrared camera ~ 5 hours after the burst trigger time. An extended object was found within the XRT error circle as reported by Aoki et al. (2006), but it is still in debate whether the object is a host galaxy of GRB 060904A or not. Konus-Wind measured the spectral peak energy as $E_p = 163 \pm 31$ keV in the 20 keV – 2 MeV energy range (Golenetskii 2006). The Wide-band All-sky Monitor (WAM) aboard *Suzaku* also detected the prompt emission (Tashiro et al. 2006). Using luminosity indicators (e.g. Amati and Yonetoku relation), a possible redshift is estimated as pseudo- $z = 1.84 \pm 0.85$ (Pelangeon & Atteia 2006). Hereafter we will assume this redshift when we discuss physical quantities measured in the rest frame of the GRB.

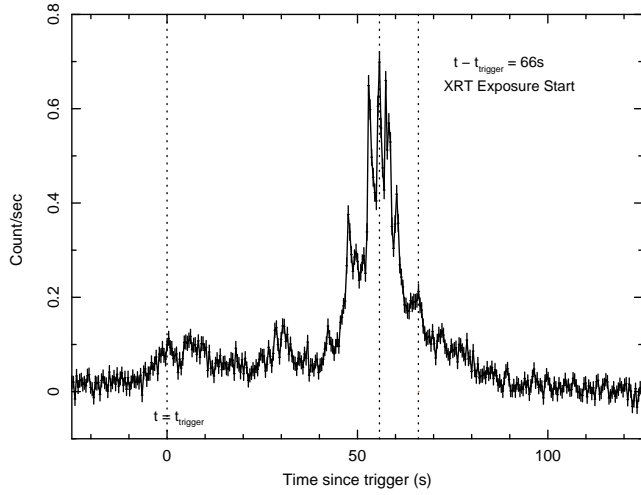


Fig. 1. The BAT lightcurve of prompt emission of GRB 060904A. The XRT follow-up observation was started at $t - t_{trigger} = 66$ sec during the prompt tail.

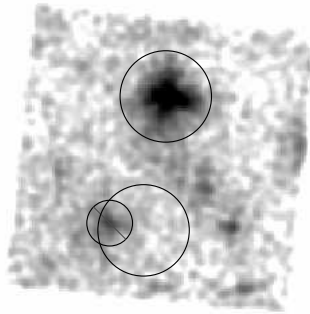


Fig. 2. The image of X-ray afterglow of GRB 060904A observed with the *Suzaku*/XIS. The brightest source in the frame is the X-ray afterglow, and we extract X-ray events within 2.89 arcmin radius as source signals. The background region is determined at the opposite side across the optical axis of the X-ray telescope. Since we found a dim source within the background region, it was removed as shown by a small circle with a diagonal line.

3. Data Reduction

The *Swift*/BAT and XRT data were analyzed by standard analysis tools within the heasoft 6.2.0 packages¹. For the windowed timing mode data of XRT, using xselect software, we extracted both X-ray afterglow and background spectra within rectangular regions of 40 pixels in width with a height large enough to include all the photons. We used the energy response matrix file (RMF) released by the XRT team, and the ancillary response file (ARF) was generated for each spectral file with the “xrtmkarf” command including the latest calibration database.

We divided the entire XRT data into 22 time intervals as shown in figure 3. Since the X-ray count rate is quite high just after the start of XRT’s pointing observation, we removed the brightest 4 pixels from the central part of the source region to deal with pile-up effects until $t - t_{trigger} \leq 86.55$ sec. As shown in the X-ray lightcurve, we can recognize 2 remarkable X-ray flares around 300 sec and 700 sec. We divided the XRT data to trace the arising and decaying behaviors for these two X-ray flares. Although the first steep decay (prompt tail) has several fluctuations in X-ray intensities, we will not discuss their temporal behavior in detail because their emission power changes are dominated by the baseline variation in the main prompt tail.

We used data resulting from processing version rev1.2 for both the *Suzaku*/XIS (Koyama et al. 2007) and HXD (Takahashi et al. 2007), and we also used the heasoft 6.2.0 packages when we performed the data reduction². For the XIS data, as shown in figure 2 we took the source region as a circle of 2.89 arcmin in radius, and the background region as the same radius from the opposite side across the optical axis of the X-ray telescope. Since we found a dim source in the background region, we removed it with smaller circle of about 2 arcmin in radius. We generated an RMF and an ARF with “xisrmfgen” and “xissimarfgen” tools including the latest calibration database, respectively. For the XIS data, we divided it into 5 time intervals and performed spectral analyses.

The 16 HXD-PINs in the well unit number of W0 are operated with bias voltage of 400 V since 2006 May 24, to suppress the rapid increase of noise events possibly caused by in-orbit radiation damage. The others were operated with a nominal bias of 500 V. Therefore we excluded the data obtained by 16 PINs in the W0 unit to avoid a large uncertainty in in-orbit calibrations. We used the non X-ray background (NXB) event data produced by the HXD team, and performed standard data reduction for remaining 48 PINs in W1, 2, and 3 units. The cosmic X-ray background (CXB) is not included in the NXB event data, so we modeled the functional form of the CXB based on past observations. The recommended RMF for a point source observed in the HXD nominal mode was adopted when we performed spectral analyses. Spectral fitting was performed using the XSPEC 12 packages for both *Swift* and *Suzaku* data. Hereafter the quoted errors are at the 90 % confidence level.

¹ <http://swift.gsfc.nasa.gov/docs/swift/analysis/>

² <http://www.astro.isas.jaxa.jp/suzaku/analysis/>

4. Spectral and Temporal Analyses

4.1. Single Power-law Fitting

We investigated spectral evolution for these 27 datasets with a simple absorbed power-law model. Hereafter, we assume galactic absorption $N_{\text{H}}^{\text{gal}} = 1.41 \times 10^{20} \text{ cm}^{-2}$ as fixed parameters (Dickey & Lockman 1990), and the extra galactic absorption $N_{\text{H}}^{\text{ext}}$ as a free parameter. We also assume a possible redshift of pseudo- $z = 1.84$ by Pelangeon & Atteia (2006). We performed spectral fitting in 0.5–10 keV for both the XRT and XIS.

In figure 4, we show the temporal histories of the X-ray energy flux in 2–10 keV band, the photon index (Γ), and the extragalactic absorption ($N_{\text{H}}^{\text{ext}}$), respectively. The temporal index of the initial steep decay phase can be described by single power-law as $(t - t_{\text{trigger}})^{-6.0 \pm 0.2}$ for the time interval No. 1–12. We can see that the flux level in the shallow decay phase is almost constant. For the late time *Suzaku* observation, we can describe the temporal decline as $(t - t_{\text{trigger}})^{-2.4 \pm 0.3}$, which is equivalent to the steeper decay phase after the jet break. Combined with *Swift* and *Suzaku* data, we can estimate a possible jet break time as $1.5 \times 10^4 < t_j < 3.8 \times 10^4 \text{ sec}$ ($0.177 < t_j < 0.440 \text{ day}$).

We can obtain acceptable fitting results for the single power-law model. However the photon indices show a remarkable and continuous softening during the prompt tail phase from $\Gamma = 1.5$ to $\Gamma = 4.8$. Starting with the first X-ray flare, the spectrum slightly became harder, and showed re-softening during its decaying phase. The photon index achieved $\Gamma = 5.30_{-0.59}^{+0.69}$ which is one of the steepest case ever observed. After the second X-ray flare, the photon indices are rapidly settled down to $\Gamma \sim 2$, which is a typical value for most X-ray afterglows, including the late time afterglow observed with *Suzaku*.

The column density $N_{\text{H}}^{\text{ext}}$ stays almost constant during the XRT observation, but we found the existence of some discrepancies between the XRT and XIS. A contamination of carbon and oxygen on the optical blocking filter of each XIS must be appropriately treated because it affects the absorption quantity in the low energy band. Although we include the contamination effect using the “xissimarfgen” tool with the latest calibration files, a systematic uncertainty exists about equivalent hydrogen column density of $6 \times 10^{20} \text{ cm}^{-2}$ in the observer’s rest frame. For a high redshift object, the systematic uncertainty of contamination should be converted by a factor of $(1 + z)^3$. Therefore the estimated column density $N_{\text{H}}^{\text{ext}}$ is influenced by a large systematic error of about $\pm 1.4 \times 10^{22} \text{ cm}^{-2}$. As a result, we can only set an upper-limit of $N_{\text{H}}^{\text{ext}} < 2.3 \times 10^{22} \text{ cm}^{-2}$ for the *Suzaku* observation. The best fit parameters are summarized in table 1.

4.2. Average Spectrum Obtained by *Suzaku*/XIS and HXD

In the previous subsection, for the *Suzaku* data, we divided the entire spectra into 5 time intervals as listed in table 1. We successfully fitted these spectra with the absorbed power-law

Table 1. Fitting results with the single power-law.

No.(Detector)	$t - t_{trigger}$ (sec)	Δt (sec)	Flux (2–10 keV) (erg/cm ² /s)	Γ	$N_{\text{H}}^{\text{ext}}$ (10 ²² cm ⁻²)	χ_{ν}^2/dof
Prompt Tail (<i>Swift</i>)						
1 (XRT+BAT)	75.3	7.5	$(1.99^{+0.24}_{-0.21}) \times 10^{-8}$	$1.51^{+0.04}_{-0.03}$	$5.10^{+0.99}_{-0.82}$	1.00/142
2 (XRT+BAT)	82.8	7.5	$(9.67^{+1.49}_{-1.23}) \times 10^{-9}$	$1.59^{+0.11}_{-0.11}$	$3.41^{+0.85}_{-0.71}$	1.12/112
3 (XRT+BAT)	90.3	7.5	$(5.11^{+0.77}_{-0.66}) \times 10^{-9}$	$1.67^{+0.13}_{-0.12}$	$2.16^{+0.62}_{-0.53}$	1.10/101
4 (XRT+BAT)	97.8	7.5	$(3.68^{+0.75}_{-0.59}) \times 10^{-9}$	$1.77^{+0.17}_{-0.15}$	$2.45^{+0.93}_{-0.72}$	0.89/69
5 (XRT)	105.3	7.5	$(2.58^{+0.50}_{-0.42}) \times 10^{-9}$	$1.95^{+0.18}_{-0.17}$	$2.62^{+0.80}_{-0.66}$	1.15/34
6 (XRT)	112.8	7.5	$(1.75^{+0.46}_{-0.35}) \times 10^{-9}$	$2.17^{+0.25}_{-0.23}$	$2.86^{+1.08}_{-0.91}$	0.76/27
7 (XRT)	124.1	15.0	$(1.02^{+0.19}_{-0.16}) \times 10^{-9}$	$2.18^{+0.21}_{-0.19}$	$1.94^{+0.63}_{-0.54}$	1.14/39
8 (XRT)	139.1	15.0	$(4.99^{+1.16}_{-0.92}) \times 10^{-10}$	$2.52^{+0.28}_{-0.24}$	$2.23^{+0.78}_{-0.65}$	1.21/26
9 (XRT)	156.6	20.0	$(2.11^{+0.53}_{-0.41}) \times 10^{-10}$	$2.89^{+0.35}_{-0.30}$	$2.35^{+0.80}_{-0.66}$	1.06/21
10 (XRT)	176.1	19.0	$(1.30^{+0.49}_{-0.34}) \times 10^{-10}$	$3.48^{+0.47}_{-0.39}$	$3.35^{+1.36}_{-1.10}$	0.95/18
11 (XRT)	200.8	30.4	$(6.74^{+1.70}_{-1.33}) \times 10^{-11}$	$3.47^{+0.43}_{-0.37}$	$2.26^{+0.78}_{-0.65}$	0.72/19
12 (XRT)	231.3	30.4	$(7.52^{+3.44}_{-2.18}) \times 10^{-12}$	$4.82^{+1.13}_{-0.88}$	$2.40^{+1.41}_{-1.05}$	0.87/14
First Flare (<i>Swift</i>)						
13 (XRT)	268.1	43.0	$(5.84^{+1.64}_{-1.17}) \times 10^{-11}$	$3.43^{+0.39}_{-0.33}$	$2.53^{+0.89}_{-0.68}$	1.25/22
14 (XRT)	311.1	43.0	$(5.79^{+1.11}_{-0.90}) \times 10^{-11}$	$3.87^{+0.33}_{-0.29}$	$2.61^{+0.59}_{-0.50}$	1.10/34
15 (XRT)	354.1	43.0	$(8.71^{+2.32}_{-1.72}) \times 10^{-12}$	$5.30^{+0.69}_{-0.59}$	$3.15^{+0.87}_{-0.71}$	1.26/21
16 (XRT)	398.6	46.0	$(4.38^{+1.61}_{-1.15}) \times 10^{-12}$	$4.50^{+1.22}_{-0.95}$	$1.52^{+1.13}_{-0.85}$	1.69/8
17 (XRT)	522.9	202	$(1.22^{+0.41}_{-0.24}) \times 10^{-11}$	$2.25^{+0.41}_{-0.27}$	$0.19^{+0.74}_{-0.19}$	1.19/10
Shallow Decay (<i>Swift</i>)						
Including Second Flare						
18 (XRT)	679.8	111	$(2.25^{+0.72}_{-0.51}) \times 10^{-11}$	$3.14^{+0.49}_{-0.40}$	$2.13^{+0.97}_{-0.74}$	0.84/17
19 (XRT)	851.8	234	$(1.88^{+0.48}_{-0.38}) \times 10^{-11}$	$2.42^{+0.35}_{-0.31}$	$1.08^{+0.69}_{-0.54}$	1.00/17
20 (XRT)	1085	234	$(1.36^{+1.12}_{-0.57}) \times 10^{-11}$	$2.25^{+0.73}_{-0.58}$	$2.76^{+3.21}_{-2.21}$	0.40/6
21 (XRT)	1377	350	$(9.33^{+4.31}_{-2.80}) \times 10^{-12}$	$2.55^{+0.50}_{-0.40}$	$2.71^{+1.86}_{-1.33}$	1.03/12
22 (XRT)	1728	352	$(9.00^{+5.06}_{-2.88}) \times 10^{-12}$	$2.81^{+0.61}_{-0.46}$	$4.08^{+2.19}_{-1.53}$	0.92/13
Late Afterglow (<i>Suzaku</i>)						
23 (XIS)	39262	2942	$(1.13^{+0.20}_{-0.15}) \times 10^{-12}$	$2.17^{+0.21}_{-0.19}$		1.06/39
24 (XIS)	45210	2551	$(7.24^{+1.89}_{-1.36}) \times 10^{-13}$	$1.93^{+0.27}_{-0.15}$		0.90/35
25 (XIS)	58234	16631	$(3.81^{+0.82}_{-0.65}) \times 10^{-13}$	$2.04^{+0.21}_{-0.18}$	< 2.30	0.99/38
26 (XIS)	74320	13365	$(1.83^{+0.53}_{-0.33}) \times 10^{-13}$	$2.10^{+0.30}_{-0.24}$		1.15/32
27 (XIS)	90868	14787	$(1.54^{+0.24}_{-0.22}) \times 10^{-13}$	$2.02^{+0.26}_{-0.20}$		1.11/31

* this value was measured from the averaged XIS spectrum. Because of the contamination effect (see text), this value has a large systematic uncertainty.

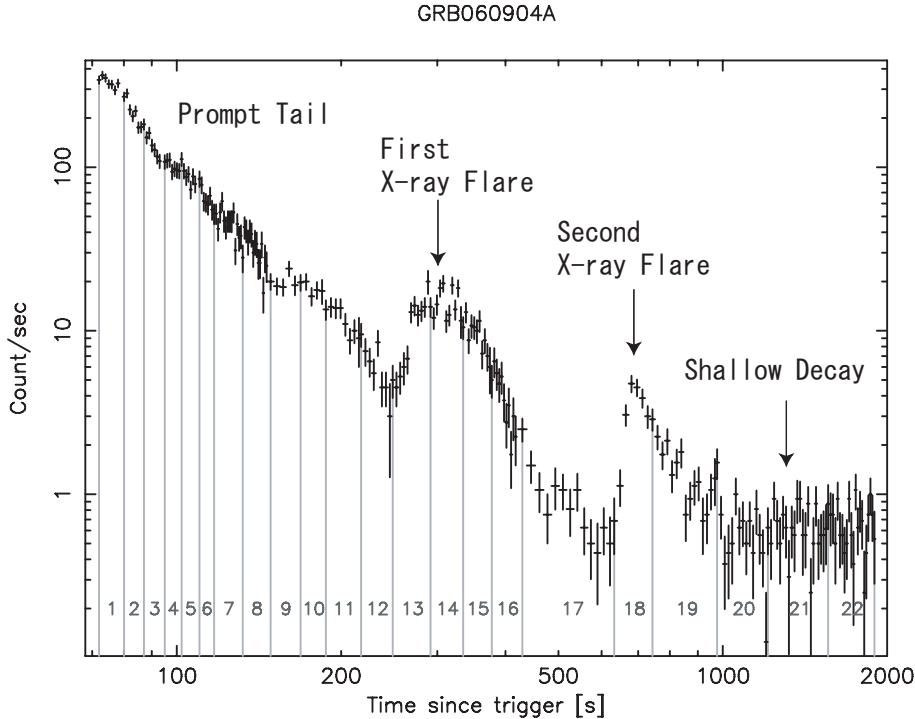


Fig. 3. The lightcurve of the early X-ray afterglow of GRB 060904A observed with *Swift*/XRT (0.5–10 keV range). We performed time resolved spectral analyses for 22 divisions as shown in this figure.

model, and found no significant spectral evolution. Therefore, we investigated the average spectrum for the late time X-ray afterglow to determine the important spectral parameters.

We also performed spectral fitting for the time averaged data from both the *Suzaku*/XIS (0.5–10.0 keV) and HXD-PIN (12–60 keV). For the HXD-PIN fitting, we subtract only the NXB from the observed data, and the CXB is included as the fixed function. A reproduction for the NXB modeling is about 4 % for the nominal HXD observations, so we include this systematics when we subtract the NXB spectrum. We used the functional form of CXB reported by Gruber et al. (1999) (see equation 1 in their paper).

We use the RMF for a point source when we fit the afterglow spectrum. However, the CXB is the extended emission, so we have to convert the CXB spectral parameters into an equivalent parameters for the RMF of point source. To do so, we simulated an expected CXB spectrum with the flat field RMF. After that, we fitted the simulated CXB spectrum with the point source RMF, and obtained the functional form as

$$\frac{dN}{dE} = 8.134 \times 10^{-4} \left(\frac{E}{1 \text{ keV}} \right)^{-1.29} \exp\left(-\frac{E}{41.13 \text{ keV}}\right) \text{ photons keV}^{-1} \text{ cm}^{-2} \text{ sec}^{-1}. \quad (1)$$

at 10–40 keV range. We used this function as the CXB spectrum.

In figure 5, we show the averaged spectrum observed with the *Suzaku*/XIS and HXD-PIN. Adopting the absorbed power-law model, we determined the photon index of $\Gamma = 2.00 \pm 0.09$ and the column density of $N_{\text{H}}^{\text{ext}} < 2.30 \times 10^{22} \text{ cm}^{-2}$ including systematic error caused by the contamination effect. The observed flux in 2–10 keV band is $F_{2-10} = (3.69 \pm 0.31) \times$

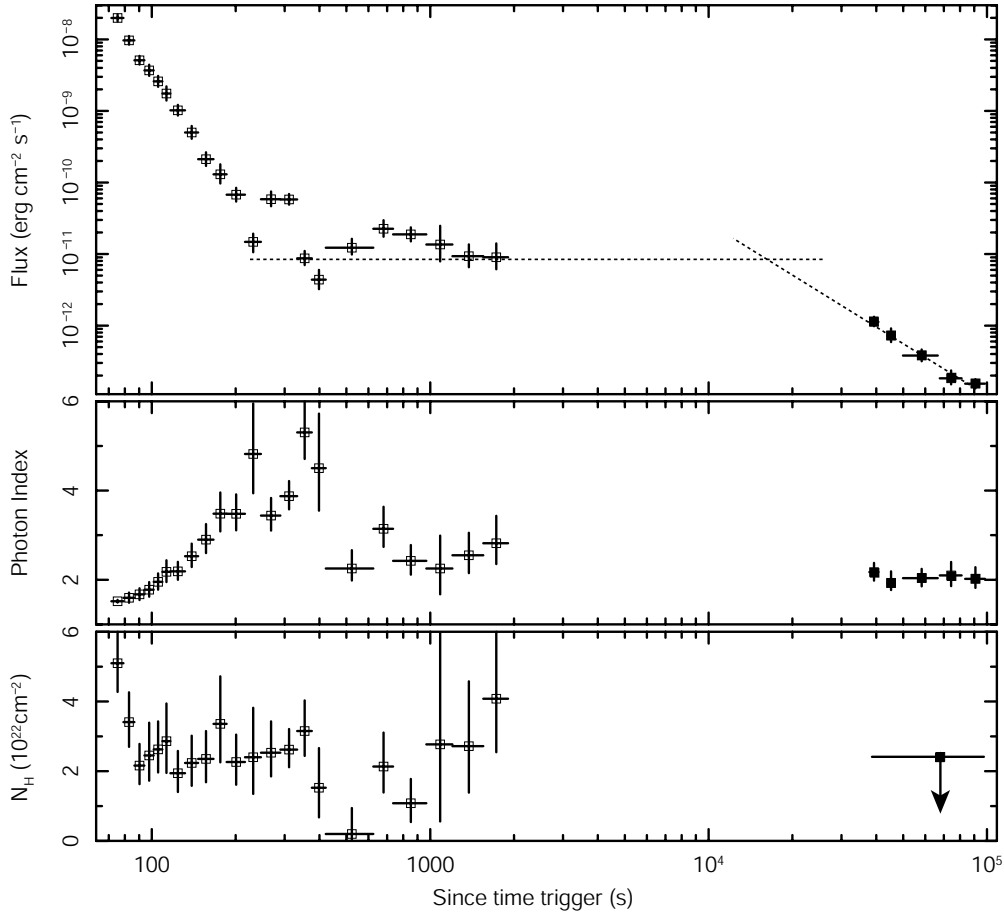


Fig. 4. The temporal histories of 2–10 keV energy flux (top), photon index (middle) and the extragalactic absorption (bottom) for the X-ray afterglow of GRB 060904A, respectively. The open and filled squares indicate the *Swift*/XRT and the *Suzaku*/XIS observations.

10^{-13} erg cm $^{-2}$ s $^{-1}$. Assuming the same photon index of $\Gamma = 2.00$ at the HXD-PIN energy band, we set the upper-limit flux in 10–40 keV band as $F_{10-40} < 1.15 \times 10^{-11}$ erg cm $^{-2}$ s $^{-1}$.

5. Advanced Spectral Analyses

In figure 6, we show several representative spectra in different time intervals on the same figure. We can clearly recognize the strong spectral softening. The flux in the harder X-ray band shows a rapid decline while below 1.0 keV there is hardly decay at all. This trend was clearly observed during the decay phase of the first X-ray flare as shown in figure 6 (right). If we assume the standard synchrotron radiation by the accelerated electrons with a power-law energy distribution ($N(\gamma_e) \propto \gamma_e^{-p}$), the energy index of photon spectrum can be described as $\nu^{-p/2}$ in the fast cooling regime. For this case, the photon index of $\Gamma = 5.3$ is equivalent to an electron energy distribution of $\gamma_e^{-8.6}$. This ultra steep index rules out this efficient acceleration any more. Although the simple power-law model is acceptable as shown in table 1, the ultra soft spectrum deviates from the standard synchrotron scenario. Some advanced spectral models

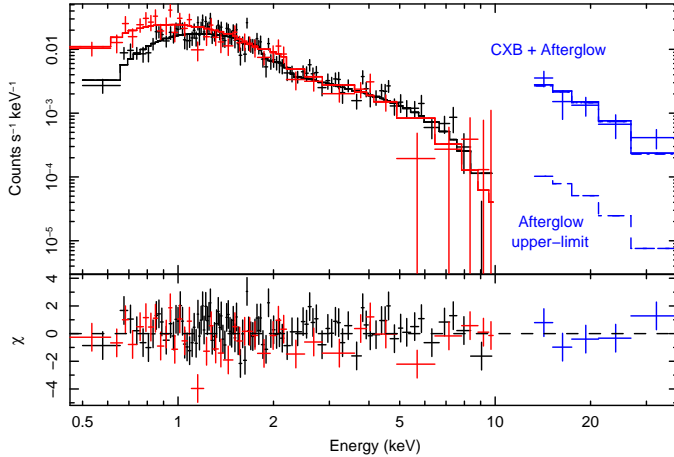


Fig. 5. The spectrum of X-ray afterglow of GRB 060904A observed by the *Suzaku*/XIS and HXD-PIN. The black and red colors indicate a summed spectrum of front-illuminated chips and one of back-illuminated chip, respectively. The blue spectrum includes the CXB component, and the upper-limit flux is described by the dotted line. Each spectrum includes its own detector responses.

may be required. In this section, we give a possible model to explain the observed softening.

The spectra of prompt emissions can be well described by the empirical Band function (Band et al. 1993), which is composed of an exponentially connected broken power-law. The accurately determined parameters of photon indices for the low and high energy band are $\alpha \sim -1$ and $\beta \sim -2.25$, respectively (Preece et al. 2000; Kaneko et al. 2006). When we notice the fitting results by the single power-law model in table 1, we can recognize that the break energy (peak energy) passes through the XRT energy window during the time interval 1–6 because the photon indices changes from $\Gamma = 1.5$ to softer value than $\Gamma = 2$. However, it is not possible to explain the very steep photon index, such as $\Gamma = 5.3$, found in GRB 060904A spectra.

Next, we performed an advanced spectral analysis using a broken power-law with exponential cutoff (BPEC) model. Here we used broken power-laws instead of the Band function because the break energy on the Band function can be determined only when $10 \leq E_0 \leq 10^4$ keV in the standard analysis package “XSPEC” while we hope to measure the break energy in the XRT band. In the BPEC model, we denote several parameters as following (see also figure 7):

1. $E^{-\Gamma_1}$: $\Gamma_1 \sim 1.5$ between $\nu_c < \nu < \nu_m$ for the fast cooling case. Here ν_c and ν_m are the frequency determined by the cooling time and the minimum electron energy, respectively. Hereafter we denote the break energy as $E_1 \equiv h\nu_m$ which corresponds to the peak energy in the Band function.
2. $E^{-\Gamma_2}$: $\Gamma_2 \sim 2.25$ at the range of $\nu > \nu_m$ for the power-law index of electron energy distribution of $p = 2.5$ (fast cooling case).
3. $\exp(-E/E_2)$: We introduce a cutoff component above the higher energy ends to describe the spectra with very steep photon indices. Several possible physical interpretations will be discussed in the following section.

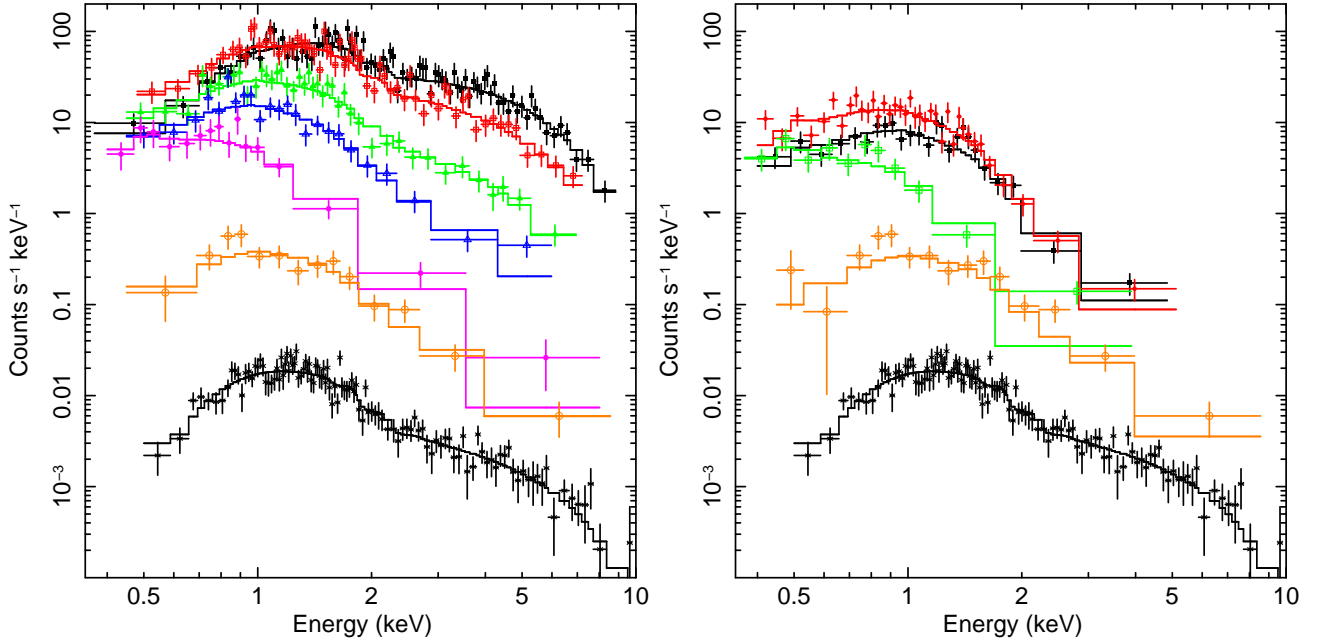


Fig. 6. The spectral evolution of early X-ray afterglow of GRB 060904A with the best fit power-law model listed in table 1. The left panel shows 7 time-resolved spectra (No.1:black, 3:red, 7:green, 9:blue, 12:magenta, 21:orange see figure 3) observed by XRT as well as the late time X-ray afterglow observed by *Suzaku*/XIS (bottom black). The right panel shows same as the left one for the X-ray flare around ~ 300 sec. Each color corresponds to the spectrum of different time intervals (13:black, 14:red, 16:green and 21:orange) with the XIS spectrum (bottom black). For clear comparison with the spectrum of shallow decay phase, we also inserted the No.21 and late afterglow spectra on these figures.

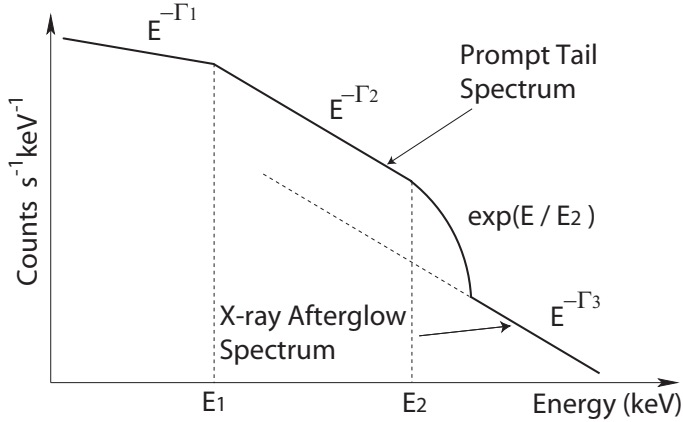


Fig. 7. A schematic view of the broken power-law and the exponential cutoff (BPEC) model.

4. $E^{-\Gamma_3}$: an additional power-law component is required to describe a steady hard spectrum of the shallow decay phase.

We succeeded in fitting 22 datasets of XRT spectra with the BPEC model. The best fit results are summarized in table 2. The blank spaces mean that the BPEC model is out of energy

range covered by the XRT. We found that E_1 (equivalent to the peak energy) passed through the XRT energy band during the time interval of No.3–5. Next, the spectra can be described by the single power-law with the photon index of $\Gamma_2 \sim 2.25$. After that, the exponential cutoff energy (E_2) got through the XRT energy window during the time interval of No.9–16. Finally, the variable prompt tail emission left the energy range below 0.5 keV, and only the X-ray afterglow in shallow decay phase was observed. The spectra obtained by the *Suzaku* observation can be well fitted by the single power-law with $\Gamma_3 \sim 2$ which have been already listed in the table 1.

We also adopted the BPEC model to the BAT data obtained before the start time of XRT observation. We used the time interval of $55 < t - t_{trigger} < 66$ s which corresponds to the tail emission phase of the most intense peak before the XRT observation start time. We succeeded in measuring the break energy of $E_1 = 112.2_{-15.7}^{+41.6}$ when we set $\Gamma_2 = 2.25$ (fix). This result strongly supports that the break energy E_1 continuously passed through from the BAT to the XRT energy ranges.

6. Afterglow Component in the Prompt Tail and the X-ray Flare

In the previous section, we divided the *Swift* and *Suzaku* data into short time intervals to investigate the detailed temporal history of spectral evolutions. The spectra of prompt tail emission significantly become softer, and we detect passage of the typical break energy through the *Swift*/XRT window. However, in these analyses, it is difficult to distinguish the X-ray afterglow from the prompt tail and/or the X-ray flare because the photon statistics at the high energy band become poor. Therefore, to improve this fact, we combined several spectra with the photon indices softer than $\Gamma > 4$ for the purpose of investigating the spectral shape up to 10 keV.

In figure 8, we show the X-ray spectrum at the merged time intervals of 12 + 15 + 16 (black), and the average spectrum of late time afterglow observed by *Suzaku* (red). For this merged spectrum, the BPEC model was rejected with the reduced chi-square value of $\chi^2_{\nu}/(\text{dof}) = 1.89/(39)$. This is because the spectrum shows a clear hardening break around 2 keV and there are large discrepancies between the data and the BPEC model function above 2 keV. To represent the observed harder spectrum beyond 2 keV, we added a single power-law model of $\propto E^{-\Gamma_3}$ to the BPEC model as described in the previous section. Then the fitting result is significantly improved as $\chi^2_{\nu}/(\text{dof}) = 1.15/(38)$. The best fit parameters are $N_{\text{H}}^{\text{ext}} = 2.24 \pm 0.25$, $E_2 = 0.29 \pm 0.06$ and $\Gamma_3 = 1.87 \pm 0.61$ with the fixed index of $\Gamma_2 = 2.25$ (the other parameters, Γ_1 and E_1 , are out of XRT range).

Therefore we can naturally recognize this spectrum includes two emission components. The BPEC model obviously represents the prompt tail spectrum, and the additional single power-law may represent the X-ray afterglow component because the photon index (Γ_3) is consistent with one of the shallow decay phase and the late time afterglow observed with *Suzaku* while the uncertainty is quite large. We succeeded in distinguishing the X-ray afterglow

Table 2. Fitting results of the broken power-law with exponential cutoff model.

No.	Data	Γ_1	E_1 (keV)	Γ_2	E_2 (keV)	Γ_3 afterglow	$N_{\text{H}}^{\text{ext}}$ (10^{22} cm^{-2})	χ^2_{ν}/dof
	Konus	$1.00^{+0.23}_{-0.17}$	163 ± 31	$2.57^{+0.37}_{-1.00}$	0.61/61
	BAT	$1.39^{+0.06}_{-0.06}$	$112.2^{+41.6}_{-15.7}$	2.25(fix)	0.68/55
1	XRT/BAT	$1.48^{+0.04}_{-0.05}$	$62.4^{+16.0}_{-17.5}$	2.25(fix)	$4.77^{+0.94}_{-0.61}$	0.96/141
2	XRT/BAT	$1.54^{+0.06}_{-0.08}$	$41.4^{+19.3}_{-16.0}$	2.25(fix)	$3.16^{+0.77}_{-0.64}$	1.16/111
3	XRT/BAT	1.50(fix)	$8.62^{+3.27}_{-2.85}$	2.25(fix)	$1.61^{+0.37}_{-0.31}$	1.06/101
4	XRT/BAT	1.50(fix)	$3.14^{+0.97}_{-0.71}$	2.25(fix)	$1.83^{+0.57}_{-0.70}$	0.96/69
5	XRT	1.50(fix)	$2.28^{+0.86}_{-0.42}$	2.25(fix)	$1.75^{+0.50}_{-0.42}$	1.18/34
6	XRT	1.50(fix)	< 1.50	$2.18^{+0.23}_{-0.23}$	$2.22^{+1.40}_{-0.93}$	0.76/26
7	XRT	1.50(fix)	< 1.42	$2.17^{+0.21}_{-0.19}$	$1.37^{+1.01}_{-0.52}$	1.14/38
8	XRT	$2.53^{+0.28}_{-0.25}$	> 5.78	$2.24^{+0.78}_{-0.66}$	1.21/25
9	XRT	2.25(fix)	$3.59^{+3.80}_{-1.41}$	$1.81^{+0.57}_{-0.47}$	1.16/21
10	XRT	2.25(fix)	$1.69^{+0.82}_{-0.49}$	$2.28^{+0.91}_{-0.75}$	0.83/18
11	XRT	2.25(fix)	$1.52^{+0.72}_{-0.46}$	$1.53^{+0.55}_{-0.46}$	0.73/19
12	XRT	2.25(fix)	$0.52^{+0.32}_{-0.17}$	$1.46^{+0.49}_{-0.77}$	0.97/14
13	XRT	2.25(fix)	$1.51^{+0.64}_{-0.41}$	$1.83^{+0.62}_{-0.48}$	1.16/22
14	XRT	2.25(fix)	$1.09^{+0.30}_{-0.23}$	$1.70^{+0.41}_{-0.35}$	1.12/34
15	XRT	2.25(fix)	$0.42^{+0.11}_{-0.08}$	$2.13^{+0.31}_{-0.28}$	0.84/21
16	XRT	2.25(fix)	$0.25^{+0.16}_{-0.10}$	2.25(fix)	$1.66^{+0.56}_{-0.52}$	1.27/8
17	XRT	$2.25^{+0.41}_{-0.23}$	< 0.94	1.19/10
18	XRT	2.25(fix)	$2.23^{+2.17}_{-0.89}$	$1.53^{+0.65}_{-0.50}$	0.91/17
19	XRT	$2.42^{+0.35}_{-0.31}$	$1.08^{+0.69}_{-0.54}$	1.00/17
20	XRT	$2.25^{+0.73}_{-0.58}$	$2.76^{+3.21}_{-2.21}$	0.40/6
21	XRT	$2.55^{+0.50}_{-0.40}$	$2.71^{+1.86}_{-1.33}$	1.03/12
22	XRT	$2.81^{+0.61}_{-0.46}$	$4.08^{+2.19}_{-1.53}$	0.92/13

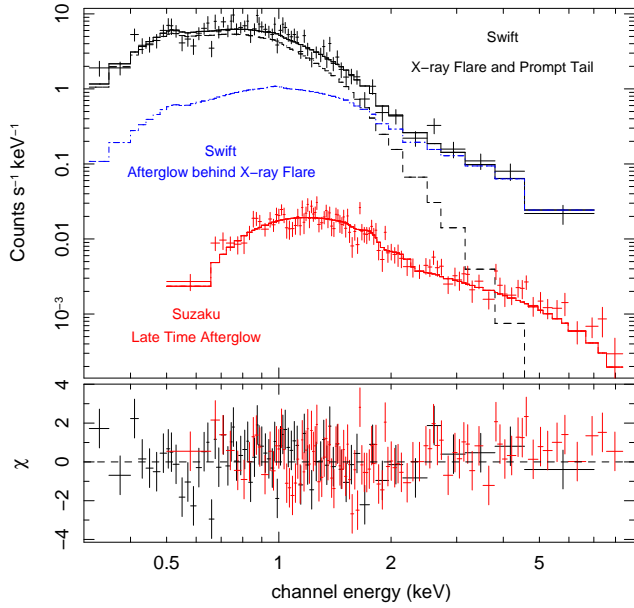


Fig. 8. A summed spectrum during the time interval with the photon index $\Gamma > 4$ (No.12+15+16). The spectrum breaks around 2 keV, and the photon index changes harder toward the higher energy band. This spectrum can be fitted with the cutoff power-law plus the single power-law model representing the prompt tail and the behind X-ray afterglow, respectively.

component from the prompt tail emission. Although the prompt tail emission shows significant spectral evolution as previously shown, the spectral slope above 2 keV is consistent with the typical absorbed power-law with the photon index of $\Gamma \sim 2$. This fact indicates that the emitter of prompt emission is due to completely different dynamics from the X-ray afterglow. We can conclude the emission sites of two distinct phenomena obviously differ from each other.

7. Discussions

We found significant spectral softening during the prompt tail emission of GRB 060904A. Moreover, we found similar spectral softening in the X-ray flare. The photon indices evolve from $\Gamma = 1.5$ to $\Gamma = 5.3$, which is one of the steepest spectra ever reported. We think there are two noticeable points to be discussed. One is a possible origin of the ultra steep spectrum and/or the exponential cutoff. And another is the time profile of the spectral break energy.

7.1. Possibility of Ultra Soft Spectra

The photon indices in the early X-ray afterglow of GRB 060904A evolves toward $\Gamma = 5.3$. This is one of the steepest case ever observed. Zhang et al. (2006) performed simultaneous studies for 17 prompt tail emissions observed by *Swift*/XRT. According to their results, 10 GRBs have significant hard-to-soft trend and the others show no spectral evolution. In this paper, we investigated two spectral models to describe the spectral softening – the simple power-law model and the broken power-law with exponential cutoff (BPEC) model. Although we obtained

acceptable results for both models, we suggest the BPEC model is better to explain the observed spectra as following reasons.

General X-ray afterglows are well fitted by a simple power-law model with a photon index of $\Gamma \sim 2$. The origin of this non-thermal spectrum is thought to be synchrotron radiation via accelerated electrons with the power-law energy distribution ($N(\gamma_e) \propto \gamma_e^{-p}$). Then we expect the power-law spectrum with the energy index of $E^{-p/2}$ for the fast cooling regime. As previously mentioned, the energy distribution of seed electrons with $\gamma_e^{-8.6}$ is required to explain the observed photon index of $\Gamma = 5.3$ by the standard synchrotron radiation. This is a really steep electron spectrum, and we may be able to recognize the existence of high energy limit of Fermi-type acceleration if we trust the synchrotron scenario. In this case the photon spectrum should be modified. The spectral shape changes the exponential function above the synchrotron frequency corresponding to the maximum energy electrons. The highest end of the BPEC model represents this situation, and it can be well adopted to the observed spectra for GRB 060904A.

In figure 9, we show the time history of the spectral break energies. The open and filled squares indicate the E_1 and E_2 profiles of the prompt tail emission, measured from the most intense peak at $t - t_{trigger} = 55$ s, respectively. The first point of open square is represented by the peak energy of $E_p = 163 \pm 31$ measured from the average spectrum observed with *Konus-Wind* (Golenetskii 2006). The open triangles are one of E_2 in the X-ray flare measured from its peak at $t - t_{trigger} = 268.1$ s. When we adopt a power-law model for each time profile, we obtained

$$E_{break} \propto \begin{cases} t^{-3.9 \pm 0.4} & \text{for } E_1 \text{ of prompt tail} \\ t^{-3.2 \pm 1.4} & \text{for } E_2 \text{ of prompt tail} \\ t^{-1.7 \pm 0.5} & \text{for } E_2 \text{ of X-ray flare.} \end{cases} \quad (2)$$

According to the time history of break energies shown in figure 9, we can recognize that the time profiles of both E_1 and E_2 in prompt tail emission are very similar to each other. This fact may lead us to consider the situation that the spectral shape is likely to be stable as the BPEC model in the rest frame of emitter, and the typical break energies cross toward the low energy band caused by some physical mechanism. When we extrapolate the cutoff energy (E_2) toward the brightest time of main emission at $t - t_{trigger} = 55$ sec, we estimate $E_2 \sim 1$ MeV which is only one order of magnitude larger than the peak energy of $E_p = 163 \pm 31$ reported by Golenetskii (2006).

7.2. Time Profile of Spectral Break Energy

Let us assume an instantaneous emission from the relativistic shell, then a delayed emission caused by a geometrical curvature of emitting material is expected. This effect is widely called as the curvature effect. The relativistic boosting of delayed emission is much smaller than one of the on-axis emission. Therefore, the characteristic frequencies of prompt

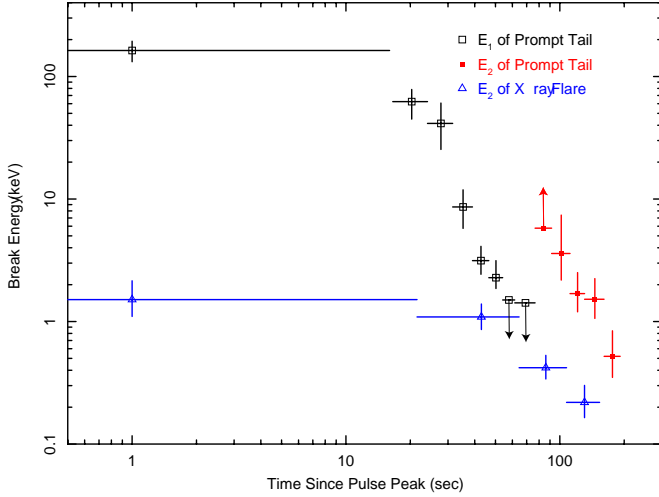


Fig. 9. Time histories of spectral break energies. The open and filled squares mean the break energy E_1 and E_2 of the prompt tail emission measured from the most intense pulse at $t - t_{trigger} = 55$ sec. The open triangles mean the E_2 history of the X-ray flare measured from $t - t_{trigger} = 268.1$. The decay profiles of E_1 and E_2 in prompt tail are very similar, and the best fit power-law model is $t^{-3.9 \pm 0.4}$ and $t^{-3.2 \pm 1.4}$, respectively.

emission, such as E_1 and E_2 in this paper, become softer as time goes by.

When we define a point where the radial velocity of expanding spherical shell is parallel to the line of sight to be $\theta = 0$, a Doppler factor (δ) toward the observer at a high latitude angle θ is given by

$$\delta = \frac{1}{\gamma(1 - \beta \cos \theta)}. \quad (3)$$

Here γ and $\beta = v/c$ are the Lorentz factor and the velocity of emitting shell, respectively. The difference of photon arrival time caused by the geometrical curvature can be described as

$$t - t_0 = \frac{R_0(1 - \cos \theta)}{c}, \quad (4)$$

where R_0 is the radius of emitting material, t_0 is the arrival time of photon emitted at $\theta = 0$, and c is the light velocity. For extremely relativistic case, we can adopt $\beta \sim 1 - 1/2\gamma^2$ and denote the Doppler factor as a function of t ;

$$\delta(t) \sim \frac{2\gamma}{1 + (t - t_0)/\tau}, \quad \tau \equiv \frac{R_0}{2\gamma^2 c}. \quad (5)$$

Then the spectral break energies are expected to have the time dependence of

$$E_{break}(t) = \frac{E_{break,0}}{1 + (t - t_0)/\tau}. \quad (6)$$

Here, the time constant τ means an angular spreading time and it is equivalent to about 1 second for the typical parameters of $R_0 \sim 10^{15}$ cm and $\gamma \sim 100$. Therefore the spectral evolution during the prompt tail at $t - t_0 \gg 1$ sec can be approximately described as $\propto (t - t_0)^{-1}$ if the curvature effect controls the spectral softening. However, we found the time history of characteristic energy E_1 and E_2 as equation 2, and they are inconsistent with the above discussions.

Let us consider the curvature effect from a different point of view. The spherical curvature effect predicts the relation of $\alpha_x = \beta_x + 2$ between the temporal index α_x and the spectral energy index $\beta_x (= \Gamma - 1)$ (Kumar & Panaitescu 2000). As shown in figure 4, the temporal index is rather stable as $\alpha_x = 6.0 \pm 0.2$ during the prompt tail while the spectral index evolves from $\Gamma = 1.5$ to $\Gamma = 5.3$ for the case of single power-law fitting. This observational fact is not satisfied with the above relation. For the fitting based on the BPEC model, it is difficult to argue the consistency or discrepancy of the $\alpha_x = \beta_x + 2$ relation, because this relation is valid only in the case where no spectral break energy crosses the observational band. Even if we assume the photon indices of pre- and post-break as $\Gamma_1 = 1.5$ and $\Gamma_2 = 2.25$, either cases can not adopt the $\alpha_x = \beta_x + 2$ relation. Therefore, we conclude it is impossible to explain the observed spectral and temporal properties by only the spherical curvature effect. We may have to consider more complicated system such as the structured jet and the multiple jets rather than the spherical uniform jet as well as hydrodynamics.

The spectra of prompt emissions are widely believed as the Band function (Band et al. 1993) with the low and the high energy photon indices of ~ -1 and ~ -2.25 , respectively. For the bright GRBs, e.g. GRB 990123, the non-thermal emissions is really extending over ~ 10 MeV (Briggs et al. 1999). Dingus (2001) reported an average spectrum of 4 GRBs detected by *CGRO*/EGRET. The spectrum really achieves 10 GeV with the photon index of $\Gamma = 1.95 \pm 0.25$. This is consistent with an extension of the electron synchrotron component. On the other hand, Preece et al. (2000) reported the spectral properties for the brightest 156 GRBs detected by *CGRO*/BATSE. In their results, about 10 % of treated spectra show the high energy indices of $\beta < -4$. Kaneko et al. (2006) independently confirmed the same property. They categorized these events showing steep spectra as a non-high energy portion.

In this paper, we showed the very steep spectra in the early X-ray afterglow, and argued the possibility of exponential cutoff at the highest part of X-ray spectrum. If this GRB 060904A and the events with spectral evolution reported by Zhang et al. (2006) belong to the non-high energy population defined by Preece et al. (2000), the fraction of inefficient acceleration cases of all GRBs may be larger than we have expected, and reaches about 50 %. Then, several physical phenomena may have to be reconsidered. This spectral evolution will be an important key to investigate the acceleration mechanism in the relativistic blast wave. We encourage the future observation with the *Swift*/BAT and XRT for early X-ray afterglows of very bright GRBs.

8. Acknowledgment

We thank R. Yamazaki, K. Ioka, T. Sakamoto and G. Sato for the useful discussions about the spectral evolution based on the curvature effect. We also thank This research was supported by Grant-in-Aid for Scientific Research of the Japanese Ministry of Education, Culture, Sports, Science and Technology, No.18684007 (DY). YEN is supported by the JSPS Research

References

- Aoki, K., Tanaka, I., Kawai, N., et al., 2006, GCN, 5522
Amati, L., et al., 2002, A&A, 390, 81
Band, D. L., Matteson, J., Ford, L., et al. 1993, ApJ, 413, 281
Briggs, M. S., et al., 1999, ApJ, 524, 1, 82
Butler, N. R., 2006, astro-ph/0604083
Dermer, C. D., 2004, ApJ, 614, 284
Dickey, J. M., & Lockman, F. J., 1999, ARAA, 28, 215
Dingus, B. L., 2001, AIPC, 558, 383
Fenimore, E. E., Madras, C. D., & Nayakshin, S., 1996, ApJ, 473, 998
Gehrels, N., Chincarini, G., Giommi, P., et al. 2004, ApJ, 611, 1005
Golenetskii S., Aptekar R., Mazets E., et al., 2006, GCN, 5518
Gruber, D. E., Matteson, J. L., & Peterson, L. E., 1999, ApJ, 520, 124
Kaneko, Y., Preece, R. D., Briggs, M. S., et al., 2006, ApJS, 166, 298
Koyama, K., et al., 2007, PASJ, 59, S23
Kumar, P. & Panaitescu, A. 2000, ApJ, 541, L51
Liang, E. W., et al. 2006, ApJ, 646, 351
Mitsuda, K., et al., 2007, PASJ, 59, S1
Nousek, J. A., et al., 2006, ApJ, 642, 389
Panaitescu, A., 2007, astro-ph/0705.1015
Pelangeon, A. & Atteia, J.-L. 2006, GCN, 5521
Piran, T., 1999, Physics Report, 314, 575
Preece, R. D., et al., 2000, ApJS, 126, 1, 19
Ryde, F., 2005, ApJ, 625, L95
Ryde, F., et al., 2006, astro-ph/0608363
Sato, G., et al., 2006, astro-ph/0611148
Takahashi, T. et al., 2007, PASJ, 59, S35
Tashiro, M. S., et al., 2006, GCN, 5543
Tashiro, M. S., et al., 2007, PASJ, 59, 361
Yamazaki, R., et al., 2006, MNRAS, 369, 311
Yonetoku, D., et al., 2004, ApJ, 609, 935
Zhang, B-B., Liang, E-W, & Zhang, B., 2006, astro-ph/0612246